Nonstoichiometric $LiFePO_4$: Defects and Related Properties

P. Axmann,[†] C. Stinner,[†] M. Wohlfahrt-Mehrens,[†] A. Mauger,*[,‡] F. Gendron,[§] and C. M. Julien[§]

Zentrum für Sonnenenergie and Wasserstoff Forschung, Helmholtzstrasse 8, 89081 Ulm, Germany, Université P. et M. Curie-Paris 6, Institut de Minéralogie et Physique des Milieux Condensés, UMR 7590, 140 rue de Lourmel, Paris 75015, France, and Université P. et M. Curie-Paris 6, Institut des Nanosciences de Paris, UMR 7588, 140 rue de Lourmel, Paris 75015, France

Received December 17, 2008. Revised Manuscript Received February 19, 2009

Deviation from ideal stoichiometry of $LiFePO_4$ has been investigated. Any attempt to increase the Li concentration of samples prepared either by the precursor precipitation route or by the continuous aqueous precursor synthesis route results in the formation of lithium phosphate impurity, in addition to stoichiometric $LiFePO_4$ free of any Li vacancy. On the other hand, Li-deficient homogeneous solid solutions of composition $Li_{1-2x}Fe_xFePO_4$ could be obtained. For $x \geq 0.06$, however, a sarcopside impurity phase is formed. Investigations of structural properties allow us to define the defect responsible for the solid solution as $Fe^{\bullet}_{Li} + V'_{Li}$ in the Kröger−Vink notation. Because the chemical formula of the sarcopside is obtained by writing $x = {}^1/_2$ in the chemical formula of the solid solution, this impurity phase can be viewed as a condensation of the $Fe^{\bullet}_{Li} + V'_{Li}$ defects. Magnetic measurements show that isolated lithium vacancies V'_{Li} are also diluted in the $Li_{1-2x}Fe_xFePO_4$ matrix. The negative charge of the isolated V'_{Li} is compensated by the valence change $Fe^{2+} \rightarrow Fe^{3+}$ of an iron ion in its vicinity, forming a small magnetic polaron that is detected by magnetic measurements. The concentration of such polarons, however, remains very small as it saturates to a concentration of 0.2−0.3 mol %, much smaller than the concentration x in V'_{Li} bound to $Fe^{\bullet}_{Li}$. The electrochemical features are significantly damaged by the $Fe^{\bullet}_{Li}$ defects that block the diffusion of lithium along the corresponding channel, while the Li_3PO_4 only acts as an inert mass.

1. Introduction

Because of its low cost, nontoxicity, and remarkable thermal stability, $LiFePO_4$ is the active cathode element of a new generation of lithium-ion batteries. This success is the result of many studies since the pioneering work of Padhi et al.[1] to reach the present state of the art where this material can now be prepared with specific capacity close to the theoretical value, 170 mAh/g. Meanwhile, the ability to prepare samples free of impurity phase opens the possibility to investigate the intrinsic properties of this material. In this context, we have recently investigated electronic transport that is driven by the small polaron hopping process.[2] This polaronic type of conductivity is usually met in glasses, but it is also met in well-crystallized $LiFePO_4$ because the material is predominantly ionic. For this reason, the electronic conductivity is very small. The solution to overcome this problem was to coat the surface of $LiFePO_4$ particles with thin layers of conductive carbon.[3] Other attempts have been envisioned, which have been discussed in ref 2. The small polaron can be viewed as a d-hole on a Fe^{3+} ion that can hop on neighboring Fe^{2+} neighbors. An important property is that this small polaron is also magnetic; that is, the d-hole on a Fe^{3+} ion spin-polarizes the neighboring Fe^{2+} ions, so that it can be detected by magnetic measurements.[4] Because an Fe^{3+} ion and thus a small magnetic polaron is induced by a Li vacancy, we have shown that the analysis of the magnetic properties allows for the quantitative determination of the concentration of Li vacancies in the samples despite the fact that Li is not magnetic.[2] This feature opens the possibility to investigate the deviation from ideal stoichiometry in relation to the mode of preparation and its effect on the electrochemical properties, which is the purpose of the present work.

The presence of Li vacancies is not surprising because the energy of formation of this defect is small.[5] This property is actually the consequence of the geometry of the olivine lattice in which $LiFePO_4$ crystallizes (Figure 1). This lattice can be viewed as an assembling of FeO_6 octahedra sharing corners forming Fe−O atomic *ac*-planes. Tetrahedral PO_4 units that are responsible for both the rigidity and the thermal stability of the lattice link these planes together and give room for Li channels along the *b*-direction.[6,7]

Defects have an important impact on the electrochemical properties. The study of small particles (40 nm) has shown

* To whom correspondence should be addressed. E-mail: alain.mauger@impmc.jussieu.fr.
[†] Zentrum für Sonnenenergie and Wasserstoff Forschung.
[‡] Institut de Minéralogie et Physique des Milieux Condensés.
[§] Institut des Nanosciences de Paris.

(1) Padhi, A. K.; Nanjundaswamy, K. S.; Goodenough, J. B. *J. Electrochem. Soc.* **1997**, *144*, 1188.
(2) Zaghib, K.; Mauger, A.; Goodenough, J. B.; Gendron, F.; Julien, C. M. *Chem. Mater.* **2007**, *19*, 3740.
(3) Ravet, N.; Chouinard, Y.; Magnan, J. F.; Besner, S.; Gauthier, M.; Armand, M. *J. Power Sources* **2001**, *97*−*98*, 503.
(4) Mauger, A.; Zaghib, K.; Gendron, F.; Julien, C. *Ionics* **2008**, *14*, 209.
(5) Islam, M. S.; Driscoll, D. J.; Fisher, C. A. J.; Slater, P. *Chem. Mater.* **2005**, *17*, 5085.
(6) Fisher, C. A. J.; Islam, M. S. *J. Mater. Chem.* **2008**, *18*, 1209.
(7) Nishimura, S.-I.; Kobayashi, G.; Ohoyama, K.; Kanno, R.; Yashima, M.; Yamada, A. *Nat. Mater.* **2008**, *7*, 707.

10.1021/cm803408y CCC: $40.75
Published on Web 03/26/2009

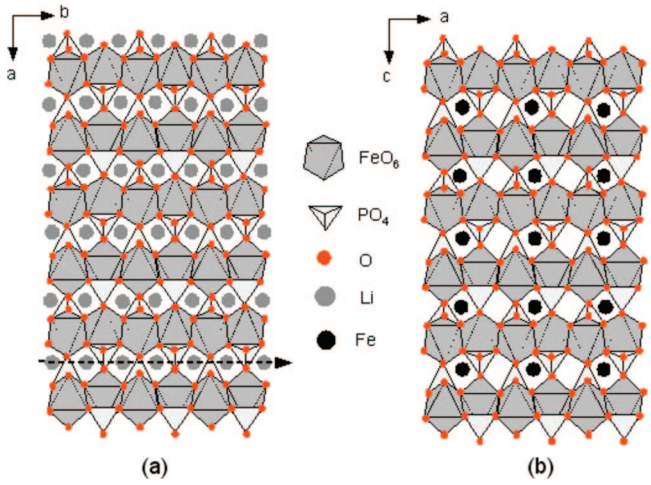

Figure 1. Structural analogy between (a) $LiFePO_4$ olivine and (b) sarcopside $Fe_3(PO_4)_2$ that can also be written $Fe_{0.5}FePO_4$ to make contact with eq 2. The dashed arrow represents the direction for lithium ions motion in the channels.

that the presence of defects or structural disorder favors the formation of the solid solution Li_xFePO_4 in the lithiation/delithiation process, instead of the phase separation between a Li-rich and Li-poor phase. This phenomenon has been observed in the surface layer (3 nm thick) alone in case the core of the particles is free of defects and well crystallized.[8,9] It has also been observed in the whole volume of the particle when not only the surface layer, but the total particle is full of defects and cation vacancies,[10] while the classical separation in two phases is recovered in case the particles (core plus surface layer) are free of defects.[1,9]

Li vacancies can be formed at the surface, and a partial deintercalation of the lithium has recently been evidenced when the surface of the particles is exposed to moisture.[11] They can also be formed in the bulk of the $LiFePO_4$ particles during the synthesis process, in which case, however, the concentration of Li vacancies and the related deviation from stoichiometry remains small (0.3% in ref 2). In these prior works, however, the synthesis process aimed at the formation of $LiFePO_4$ as close to the stoichiometry as possible. In the present work, we have selected a series of samples prepared from wet-chemical synthesis with deviations from stoichiometry (few mol % Li deficiency or excess among the precursors), with two different synthesis routes: the precursor precipitation route and the continuous aqueous precursor synthesis route.[12] We find that excess in lithium only results in Li_3PO_4 impurity phase segregation, in addition to the $LiFePO_4$ phase that remains stoichiometric. On the other hand, Li deficiency results in the formation of a homogeneous solid solution that is Li deficient due to a complex defect that is identified and does not reduce to a simple Li vacancy. These results are also discussed.

2. Experimental Section

2.1. Synthesis. $LiFePO_4$ samples of different deviations from ideal stoichiometry were synthesized using wet chemistry. Composites of Fe(II) phosphate and lithium phosphate are coprecipitated at room temperature by combining and stirring of $FeSO_4$, H_3PO_4, and LiOH solutions in appropriate amounts. The lithium phosphate content was adjusted by using various amounts of LiOH. The precipitate was filtrated, washed several times with distilled water, and mixed with lactose solution as a carbon precursor. The amount of lactose was selected to obtain a theoretical amount of 1 wt % of carbon in the final product. All process steps were performed under a nitrogen atmosphere to exclude oxidation of the precursor. The dried precursors were heat treated at 725 °C under nitrogen for 12 h.

2.2. Structural Characterization. X-ray diffraction (XRD) profiles of the samples were obtained with a Siemens D5000 diffractometer (Cu Kα radiation). Structural parameters were determined by Rietveld refinement of diffraction profiles with the TOPAS 2.1 from Bruker AXS. In addition, excess and deficiency in lithium have been determined by inductive coupled plasma (ICP) spectrometry. The apparatus was a Spectroflame Modula S: sequential scanning ICP-OES, running a 20 mm torch, 1200 W incident power, an MDSN nebulizer with 1.14 mm peristaltic pump tubing. FTIR absorption spectra were recorded with a Fourier transform interferometer (model Bruker IFS113v) in the wavenumber range 150−1400 cm^{-1} at a spectral resolution of 2 cm^{-1}. The samples were ground to fine powders and dispersed onto a CsI pellet in the proportion 1:300.

2.3. Magnetic Characterization. Magnetic measurements (susceptibility and magnetization) were carried out with a fully automated magnetometer (MPMS-5S from Quantum Design) with an ultrasensitive Superconducting QUantum Interference Device (SQUID) in the temperature range 4−300 K. Powders were placed into a small plastic vial, put into a holder, and finally inserted into the helium cryostat of the SQUID apparatus.

2.4. Electrochemical Characterization. For electrode preparation, 20 wt % of conductive carbon and 10 wt % of PTFE powder were added to the lithium iron phosphate powder and mixed in an agate mortar, rolled into flakes, and pressed into strips of aluminum grid. Each strip was mounted as positive electrode versus counter and reference electrodes of lithium metal in a glass cell and filled with a liquid electrolyte (UBE 1 M $LiPF_6$ in EC:DMC 1:1). Assemblage of the cells and electrochemical measurements were performed in an argon box. The cells were galvanostatically cycled at room temperature between 2.9 and 4.0 V vs Li/Li^+ at a specific current of *C*/20.

3. Results and Discussion

3.1. Structural Properties. The compositions deduced from ICP and XRD analyses are reported in Table 1 for three samples chosen as representative of the samples prepared with Li excess (sample L028) and Li deficiency (samples L004, L005). These are also the samples chosen to illustrate the optical and magnetic properties in this work.

For samples prepared with a Li excess, the XRD patterns are the superposition of the diffractogram of the orthorhombic olivine-type phase $LiFePO_4$ plus extra lines associated with

(8) Zaghib, K.; Mauger, A.; Gendron, F.; Julien, C. M. *Chem. Mater.* **2008**, *20*, 462.
(9) Zaghib, K.; Mauger, A.; Gendron, F.; Julien, C. M. PRIME Pacific Rim Meeting on Electrochemical and Solid-State Science, Honolulu, HI, 2008.
(10) Gibot, P.; Casas-Cabanas, M.; Laffont, L.; Levasseur, S.; Carlach, P.; Hamelet, S.; Tarascon, J.-M.; Masquelier, C. *Nat. Mater.* **2008**, *7*, 741.
(11) Zaghib, K.; Dontigny, M.; Charest, P.; Labrecque, J. F.; Guerfi, A.; Kopec, M.; Mauger, A.; Gendron, F.; Julien, C. M. *J. Power Sources* **2008**, *185*, 698.
(12) Arnold, G.; Garche, J.; Hemmer, R.; Ströbele, S.; Vogler, C.; Wohlfahrt-Mehrens, M. *J. Power Sources* **2003**, *119*, 247.

Table 1. Results of the ICP and XRD Analyses of the Samples Representative of Samples with Deficit of Lithium (L005 and L004) and Excess of Lithium (L028)[a]

		L005	L004	L028
ICP	Li_3PO_4 (mol %)	−6.8	−3.7	+18
	Li(ex)/PO_4(ex)	3.0		2.6
XRD	$LiFePO_4$	95%	100%	81%
	Li_3PO_4 (mol %)	0%	0%	19%
	$Fe_3(PO_4)_2$ (mol %)	5%	0%	0%
	V (Å^3)	291.61	291.10	290.99
discharge capacity (mAh/g)		53	115	137

[a] The discharge capacity is also reported in the last line. The negative value in the first line for the L005 and L004 samples is the value of x in $Li_{1+2x}Fe_{1-x}PO_4$, while the positive value for L028 is the value of x in the formula $LiFePO_4 + xLi_3PO_4$, as explained in the text. The second line is the ratio of concentrations of the Li in excess, Li(ex), and PO_4 in excess, PO_4(ex). Both Li(ex) and PO_4(ex) are deduced by comparison between the concentration of Li and PO_4 with that of Fe. For the sample L004 where PO_4(ex) is the order of 1%, the experimental uncertainty becomes too large to get a reliable value for the ratio Li(ex)/PO_4(ex). On the other hand, for the other samples, this ratio can be determined, and the value is found in agreement with the value 3.0 expected for the chemical formula above mentioned, within experimental uncertainty (±0.5).

Li_3PO_4. This is illustrated in Figure 2 for sample L028. No other impurity phase is detected. The volume of the unit cell and amount of Li_3PO_4 deduced from Rietveld refinement are reported in Figure 3, which shows that the volume of the unit cell is independent of the amount of Li_3PO_4. This lack of correlation shows that the material is biphased; that is, a material with y mol % excess is

$$LiFePO_4 + yLi_3PO_4 \quad (1)$$

not to be confused with a solid solution of chemical composition $Li_{1+3y}Fe(PO_4)_{1+y}$ that does not exist. The excess in Li_3PO_4 deduced from the ICP analysis is found to be in quantitative agreement with the result of the Rietveld refinement on the diffractograms (Table 2).

On the other hand, the XRD analysis of the Li-deficient samples gives evidence of an increase of the electron density on lithium positions of the olivine lattice, which can be attributed to the presence of iron ions on Li sites. The Rietveld refinement illustrated in Figure 4 also proves that the lattice parameters vary essentially linearly as a function of the deviation from stoichiometry, so that the samples are now solid solutions. This is also illustrated in Figure 3. After the Rietveld refinement (Table 3) and the ICP analyses, the compositions of the Li-deficient samples take the following form:[13]

$$Li_{1-3x}Fe(PO_4)_{1-x} \text{ or } Li_{1-2x}Fe_xFePO_4 \ (x \geq 0) \quad (2)$$

From a mathematical point of view, these two formula are equivalent only in a series development $1/(1-x) \approx (1+x)$ restricted to first order in x. However, the deviation from stoichiometry remains small (few mol %), so the difference that is in x^2 does not exceed the mol %: neither the XRD nor the ICP analyses is accurate enough to separate between these two formulas.

The first formula in eq 2 is in continuity of the former case of Li excess and eq 1, in the sense that the relative proportions of the Li, Fe, and PO_4 are the same as in the formula $LiFePO_4 - xLi_3PO_4$, which can be viewed as a deficit in Li_3PO_4.[13,14] This formulation, however, is somewhat misleading because the material is a homogeneous solution, and it is simply due to the choice of iron as the reference to determine the concentration in the other constituent Li and PO_4 units with respect to it. From a physical point of view, however, PO_4 is the stable molecular unit that can neither be moved nor broken, because of the strong P−O covalent bonding, so that it must be chosen as the reference to determine the composition of the solid solution. This choice leads to the second formula of eq 2 and shows that the intrinsic defect associated with the Li deficiency is a complex made of one Fe^{2+} ion on a Li^+ site plus a Li vacancy. In the Kröger−Vink notation, this defect is thus

$$Fe^{\bullet}_{Li} + V'_{Li} \quad (3)$$

The presence of Fe on a Li site has previously been observed in samples prepared by hydrothermal route when the temperature T chosen for the synthesis is lower than 200 °C.[15,16] In that case, it has been noticed that the iron disorder was due to Fe on a Li site while Li on a Fe site was not observed, in agreement with eq 3, and the effect of the defect on the volume of the unit cell is also the same as in our samples. Although the association of $Fe^{\bullet}_{Li}$ with Li vacancy was not mentioned in refs 15 and 16, we can then presume that the defect observed upon decreasing T in hydrothermal synthesis is the same as the defect observed in the present work. It also means that the decrease of T in the hydrothermal process leads spontaneously to a Li deficiency that is generated here by the appropriate choice of synthetic parameters.

The defect in eq 3 is neutral, and so are the chemical formulas in eqs 1 and 2. This is actually not trivial, because electronics have developed due to the fact that doping of not-so-polar semiconductors by aliovalent species is possible. $LiFePO_4$, however, is not a regular semiconductor: it is an ionic compound. It means that the cost in Coulomb energy opposes the formation of any impurity complex that would not be neutral, because the bare Coulomb potential cannot be screened.[2] In particular, Chung et al.[17] raised considerable interest and controversy by claiming that low-level doping by a range of Mg^{2+}, Al^{3+}, Ti^{4+}, Zr^{4+}, Nb^{5+} aliovalent ions increased the electronic conductivity by a factor of 10^8. In these cases, however, subsequent works have shown the increase in the electronic conductivity is actually not a doping effect, but it is simply due to a carbon coating coming from carbon-containing precursors, or due to the formation of a nanonetwork of metal-rich phosphides.[18] The full calculation of the electronic structure of the defects and their energy of

(13) Wohlfahrt-Mehrens, M. Focused Technology workshop II, Olivines in Lithium Batteries and ICMAT, Singapore, 2007.
(14) Axmann, P.; Stroebele, S.; Arnold, G.; Stinner, C.; Wohlfahrt-Mehrens, M. 11th EuroConference on Science and Technology of Ionics, Batz-sur-Mer, 2007.
(15) Chen, J.; Whittingham, M. S. *Electrochem. Commun.* **2006**, *8*, 855.
(16) Yang, S.; Song, Y.; Zavalij, P. Y.; Whittingham, M. S. *Electrochem. Commun.* **2002**, *4*, 239.
(17) Chung, S. Y.; Bloking, J. T.; Chiang, Y. M. *Nat. Mater.* **2002**, *1*, 123.
(18) Herle, P. S.; Ellis, B.; Coombs, B N.; Nazar, L. F. *Nat. Mater.* **2004**, *3*, 147.

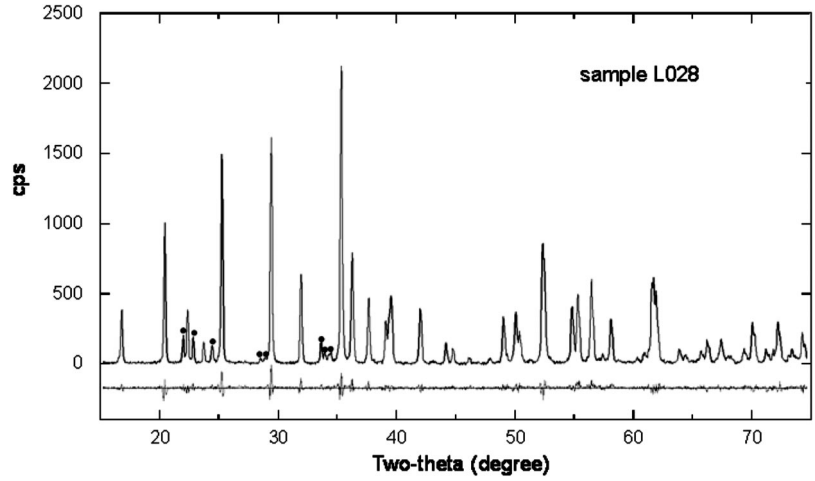

Figure 2. XRD and Rietveld refinement for sample L028. Extra lines corresponding to the Li_3PO_4 impurity are marked by dots.

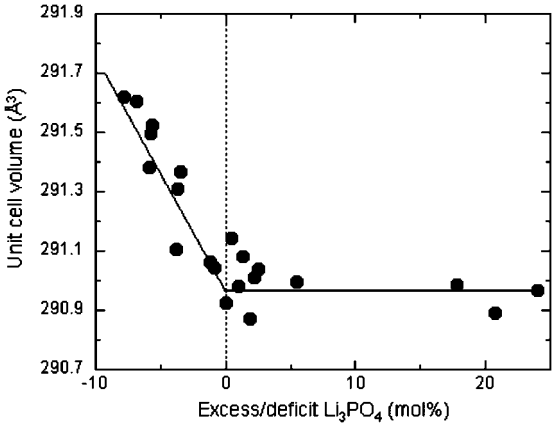

Figure 3. Unit cell volume as a function of the excess/deficit of Li_3PO_4. The solid lines are guides for the eyes. The abscissa describes the deviation x of the ideal stoichiometry by the formula $Li_{1+2x}Fe_{1-x}PO_4$ for $x < 0$ and by $LiFePO_4 + xLi_3PO_4$ for $x > 0$.

formation confirms that doping $LiFePO_4$ by the introduction of these ions is not possible.[5,19] The energy of formation is too high, and these metallic ions will precipitate. Note that, eventually, the presence of these metallic precipitates will improve the interparticle electronic conductivity, as it has been observed in ref 17. Nevertheless, none of the elements above cited will be of any help to improve the electronic conductivity inside the $LiFePO_4$ particle itself. On another hand, a recent attempt has been made to dope $LiFePO_4$ with Na instead of the elements above cited. The preliminary results suggest that a small concentration ($\leq 4\%$) of Na^+ ions might come in substitution to Fe^{2+}, in which case Na should play the role of a dopant.[20] This is presently the only potential doping element, which shows the difficulty to dope this material, and native defects in the material are then expected to be neutral to minimize the Coulomb energy.

Yet the charge neutrality in case of Li deficiency could be achieved simply by changing the valence of a neighboring iron ion from Fe^{2+} to Fe^{3+}. This defect is actually the magnetic polaron evidenced in ref 2 that corresponds to a solid solution $Li_{1-x}FePO_4$ with, however, a very small value of $x = 0.003$. An important result of the present work is that, for larger Li deficiencies, the defect that is generated to accommodate the Li deficiency in the solid solution keeps the charge neutrality with conservation of the valence of iron in the Fe^{2+} configuration. Both ICP and the Rietveld refinement of the XRD show unambiguously that the chemical composition of the Li-deficient samples is that of eq 2, not $Li_{1-x}FePO_4$. Actually, an homogeneous solution $Li_{1-x}FePO_4$ is not stable at room temperature, hence the two phases $(1-x)LiFePO_4 + xFePO_4$ obtained upon delithiation of $LiFePO_4$ at room temperature.[21,22] For a review on the lithiation/delithiation process, see ref 22 and references therein. The investigation of the phase diagram at room temperature shows that the $Li_{1-x}FePO_4$ exists only in a small range of composition $x < \varepsilon$, where ε is the solubility limit. The value of ε, however, is subject to controversy. Some works suggest $\varepsilon = 0$.[23] To the opposite, one work reports a large value $\varepsilon = 0.11$,[24] but most works report a much smaller value.[25,26] We have determined recently that the spread of this parameter over this wide range is an artifact due to the degree of disorder of the surface layer, which is not amorphous, but has a large concentration of defects reducing the lattice coherence length that is smaller than in the core of the particle, and depends strongly on the conditions of preparation and synthesis route of the material.[8,9] Because the disorder favors the homogeneous solution, the solid solution is stabilized inside the surface layer when this layer is not properly crystallized.[8,9] Therefore, the value of ε has been overestimated in prior works in which the analysis was performed assuming that the samples were homogeneous,

(19) Fischer, C. A. J.; Hart-Prieto, V. M.; Islam, M. S. *Chem. Mater.* **2008**, *20*, 5907.
(20) Yang, X.; Wang, X.; Yoon, W.; Nam, K.; Li, H.; Huang, X.; Chen, L.; Lee, H.; Breen, Mc. Abstract no. 598, PRIME 2008 Meeting, Honolulu, HI, 2008.
(21) Yamada, A.; Koizumi, H.; Nishimura, S.-I.; Sonoyama, N.; Kanno, R.; Yonemura, M.; Nakamura, T.; Kobayashi, Y. *Nat. Mater.* **2006**, *5*, 357.
(22) Ramana, C. V.; Mauger, A.; Gendron, F.; Julien, C. M.; Zaghib, K. *J. Power Sources* **2009**, *187*, 555.
(23) Yamada, A.; Kudo, Y.; Liu, K.-Y. *J. Electrochem. Soc.* **2001**, *148*, A1153.
(24) Srinivason, V.; Newman, J. *J. Electrochem. Soc.* **2004**, *151*, A1517.
(25) Yamada, A.; Koizumi, H.; Sonoyma, N.; Kanno, R. *Electrochem. Solid-State Lett.* **2005**, *8*, A409.
(26) Fischer, C. A. J.; Hart-Prieto, V. M.; Islam, M. S. *Chem. Mater.* **2008**, *20*, 5907.

Table 2. Results of Rietveld Refinement for Sample L028[a]

site	Wyck.	*x*	*y*	*z*	atom	occ.	beq
Li1	4*a*	0	0	0	Li^{1+}	0.9967(31)	1
					Fe^{2+}	0.0033(31)	1.324(72)
Fe1	4*c*	0.28233(17)	0.25	0.97417(49)	Fe^{2+}	1	1.324(72)
P1	4*c*	0.09465(33)	0.25	0.41702(73)	P	1	1.33(10)
O1	4*c*	0.09803(80)	0.25	0.7446(16)	O^{2-}	1	1.56(10)
O2	4*c*	0.45296(95)	0.25	0.2083(15)	O^{2-}	1	1.56(10)
O3	8*d*	0.16663(69)	0.04377(95)	0.28277(93)	O^{2-}	1	1.56(10)

[a] L028, phase $LiFePO_4$, space group *Pnma*(62). R-Bragg = 2.187. *a* (Å) = 10.32421(29), *b* (Å) = 6.00615(19), *c* (Å) = 4.69268(16), *V* (Å^3) = 290.987(16). $LiFePO_4$ (%) = 87.48(28), Li_3PO_4 (%) = 12.52(28).

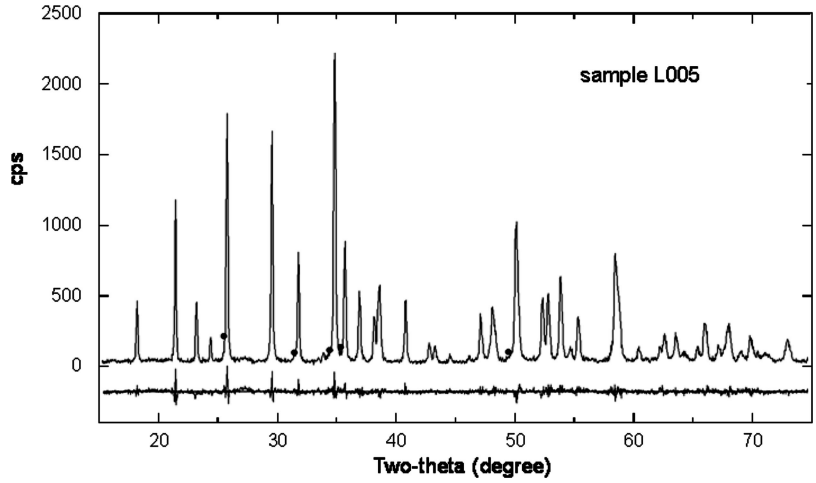

Figure 4. XRD and Rietveld refinement for sample L005. Extra lines corresponding to the $Fe_3(PO4)_2$ impurity are marked by dots.

Table 3. Results of Rietveld Refinement for Sample L005[a]

site	Wyck.	*x*	*y*	*z*	atom	occ.	beq
Li1	4*a*	0	0	0	Li^{1+}	0.9677(39)	1
					Fe^{2+}	0.0323(39)	1.231(83)
Fe1	4*c*	0.28209(20)	0.25	0.97391(56)	Fe^{2+}	1	1.231(83)
P1	4*c*	0.09378(41)	0.25	0.41718(56)	P	1	1.55(12)
O1	4*c*	0.10010(93)	0.25	0.7470(19)	O^{2-}	1	1.44(12)
O2	4*c*	0.4550(11)	0.25	0.2087(17)	O^{2-}	1	1.44(12)
O3	8*d*	0.16856(83)	0.0435(11)	0.2824(11)	O^{2-}	1	1.44(12)

[a] L005, phase $LiFePO_4$, space group *Pnma*(62). R-Bragg = 2.014. *a* (Å) = 10.32910(43), *b* (Å) = 6.00389(27), *c* (Å) = 4.70192(22), *V* (Å^3) = 291.589(22). $LiFePO_4$ (%) = 92.22(72), $Fe_3(PO_4)_2$ (%) = 7.78(72).

as they attributed the existence of the solid solution to an intrinsic effect, while it was simply due to uncontrolled defects and structural disorder. The result of the present work supports this conclusion,[8,9] because we find that $Li_{1-x}FePO_4$ is unstable already for $x = 1\%$, so that $\varepsilon < 1\%$. Beyond this limit, the complex $Fe^{\bullet}_{Li} + V'_{Li}$ is formed, so that the chemical formula switches to $Li_{1-2x}Fe_xFePO_4$ or, in closed form, $Li_{1-2x}Fe_{1+x}PO_4$. Yet, the limit of solubility for this complex defect is only $x_c \approx 0.06$. Any attempt to increase this defect concentration above this limit results in the formation of $Fe_3(PO_4)_2$ impurity phase, observed by XRD and ICP analysis (see Table 1). Note the formation of this impurity phase can be viewed as the precipitate of defects in eq 3. This feature is illustrated in Figure 1, where the sarcopside $Fe_3(PO_4)_2$ lattice is illustrated in parallel with that of $LiFePO_4$ olivine. This situation is illustrated by the sample L005. This sample is made of 5 mol % of sarcopside impurity and 95 mol % of $Li_{1-2x}Fe_xFePO_4$ with a defect concentration $x = 0.068$. This is consistent with the upper limit 7−8 mol % of iron on a Li site found in materials grown by hydrothermal process at 120 °C.[15,16]

In the spirit of eq 3, a solid solution in case of Li excess would have required the formation of the neutral defect:

$$Li'_{Fe} + Li^{\bullet}_{I} \tag{4}$$

The fact that we did not observe the defect represented in eq 4 is evidence that its energy of formation is actually so large that it cannot be generated during the synthesis process. The consequence is that the lattice cannot accommodate the excess of lithium and form a solid solution, so that the lithium in excess precipitates in the Li_3PO_4 impurity phase we have observed.

Our experimental results also clearly evidence a strong asymmetry in the Li−Fe exchange of ions; that is, few at. % Fe on Li sites can be observed, but not Li on Fe sites. This result is in agreement with the prior structural analysis of samples prepared by hydrothermal route,[15,16] while we do not have any evidence of this defect neither in our samples nor in prior works, and this disparity also makes questionable the observation of any Li−Fe antisite pair. This is the defect that was found to have the smallest energy of formation,[5] but this work only considered defects that do not modify

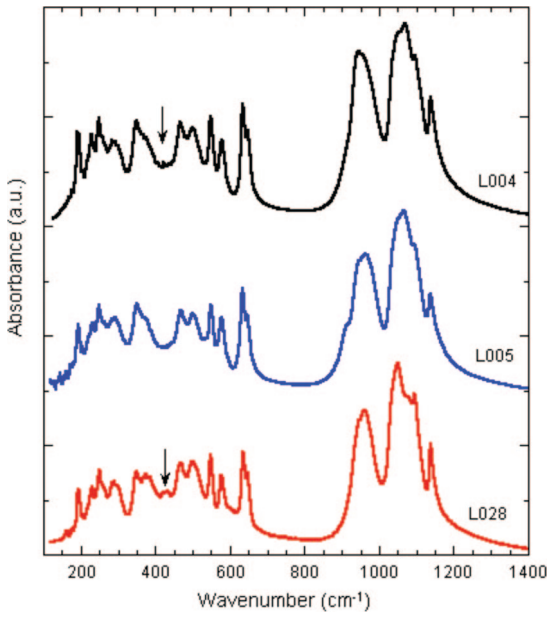

Figure 5. FTIR spectra of the three samples identified in the text. All of the bands are characteristics of the FTIR spectrum of $LiFePO_4$, except the band marked by an arrow that is the signature of Li_3PO_4 in the L028 sample.

the stoichiometry, in contrast with the defects investigated here. More recently, the association or binding energy for the pair $Fe^{\bullet}_{Li} + V'_{Li}$ has been evaluated and found to be ca. −0.5 eV,[26] which favors the formation of this defect in eq 3. Our experimental results according to which this association is indeed observed are then consistent with these calculations. On the other hand, the antisite pair was still found the most favorable intrinsic defect.[27] Note, however, that the amount of this defect, if any, will be dependent on the synthesis process, and in the present case the conditions of synthesis have been chosen to favor defects that do not conserve stoichiometry. Yet, the antisite pair has not been observed so far, to our best knowledge. Recently, STEM imaging has made possible the observation of bright contrast in Li channels, giving evidence of the presence of $Fe^{\bullet}_{Li}$, in concentration of about 1%, which is consistent with the present work.[27] Yet, this technique does not permit the observation of Li'_{Fe}.

3.2. Infrared Spectroscopy. The FTIR spectra of the selected samples are reported in Figure 5. The vibrational motions of $LiFePO_4$ and the position of the corresponding IR peaks have already been identified and discussed.[28,29] The spectra are very rich, because the vibrations of the PO_4^{3-} units are split in many components due to the correlation effect induced by the coupling with Fe−O units in the material. As we stated earlier, the richer spectrum gives evidence that the samples are well crystallized; otherwise, the bands are broadened by the reduction of the lifetime of the phonons.[30] All of the samples in Figure 5 match the spectrum observed for well-crystallized samples that have

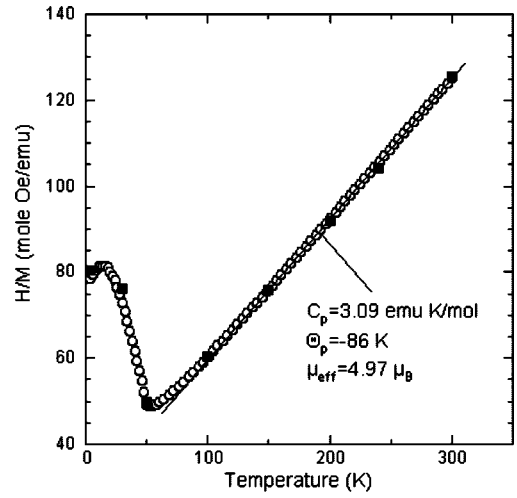

Figure 6. Inverse of the magnetic susceptibility of the L028 sample expressed in emu per mole of $LiFePO_4$, that is, after correction for the presence of Li_3PO_4 in the sample (see the text).

the full energy capacity,[31] except that the L028 sample has an extra band at 412 cm^{-1}, which is the signature of Li_3PO_4 impurity.[32] This result corroborates the presence of this impurity phase that is evidenced on this sample by the structural properties in the previous section and its absence in Li-deficient samples.

3.3. Magnetic Measurements. The magnetization $M(H)$ of the sample L028 (non reported) is linear in the magnetic field up to $H = 30$ kOe at any temperature $4 < T < 300$ K, so that the material is free from the γ-Fe_2O_3 and Fe_2P impurity phases that can poison $LiFePO_4$.[30,33] Therefore, we can define the intrinsic magnetic susceptibility χ as the ratio M/H. Note the material has a composition given in eq 1, which can be normalized as

$$(1 - y)LiFePO_4 + yLi_3PO_4 \qquad (5)$$

with $y = 1/(1 + x)$. Beccause the magnetic susceptibility of Li_3PO_4 is negligible with respect to that of $LiFePO_4$, the magnetic susceptibility of the $LiFePO_4$ part can be simply extracted by attributing the whole magnetization M to the fraction $(1 - y)$ of $LiFePO_4$. Using the result of structural analyses $(1 - y) = 0.815$, for this particular sample (see Table 1), we can then determine the magnetic susceptibility $\chi(T)$ per mole of $LiFePO_4$, or its inverse that is the quantity reported in Figure 6 to illustrate the Curie−Weiss law. The effective magnetic moment μ_{eff} per Fe ion deduced from the Curie−Weiss law $\chi = C/(T + \theta)$ above the Néel temperature $T_N = 52$ K is 4.97 μ_B, which is in very good agreement with the theoretical value 4.9 μ_B expected for Fe^{2+} in this material,[34] and observed in pure and stoichiometric $LiFePO_4$.[2] In particular, it shows that there is essentially no lithium vacancy in the material,[2] a result that was expected due to the excess of lithium in the preparation process for this sample.

(27) Chung, S.-Y.; Choi, S.-Y.; Yamamoto, T.; Ikuhara, Y. *Phys. Rev. Lett.* **2008**, *100*, 125502.
(28) Paques-Ledent, M. T.; Tarte, P. *Spectrochim. Acta, Part A* **1974**, *30*, 673.
(29) Burma, C. M.; Frech, R. *J. Electrochem. Soc.* **2004**, *151*, 1032.
(30) Ait-Salah, A.; Mauger, A.; Julien, C. M.; Gendron, F. *Mater. Sci. Eng., B* **2006**, *129*, 232.
(31) Julien, C. M.; Zaghib, K.; Mauger, A.; Massot, M.; Ait-Salah, A.; Selmane, M.; Gendron, F. *J. Appl. Phys.* **2006**, *100*, 63511.
(32) Ait-Salah, A.; Jozwiak, P.; Zaghib, K.; Garbarczyk, J.; Gendron, F.; Mauger, A.; Julien, C. M. *Spectrochim. Acta, Part A* **2006**, *65*, 1007.
(33) Julien, C. M.; Mauger, A.; Ait-Salah, A.; Massot, M.; Gendron, F.; Zaghib, K. *Ionics* **2007**, *12*, 21.
(34) Santoro, R.; Newnham, R. E. *Acta Crystallogr.* **1967**, *22*, 344.

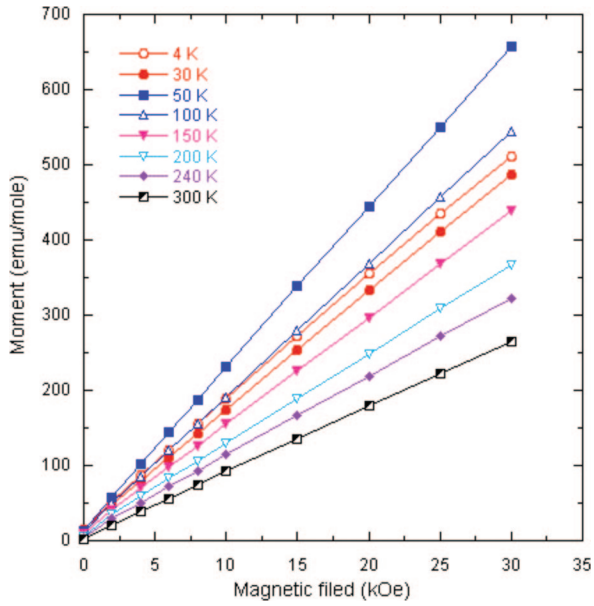

Figure 7. Magnetization curves for L004 sample. The nonlinearity below 200 K is due to nanoparticles of Fe_2P. The concentration of Fe_2P in the sample, however, is very small (≤0.1 mol %).

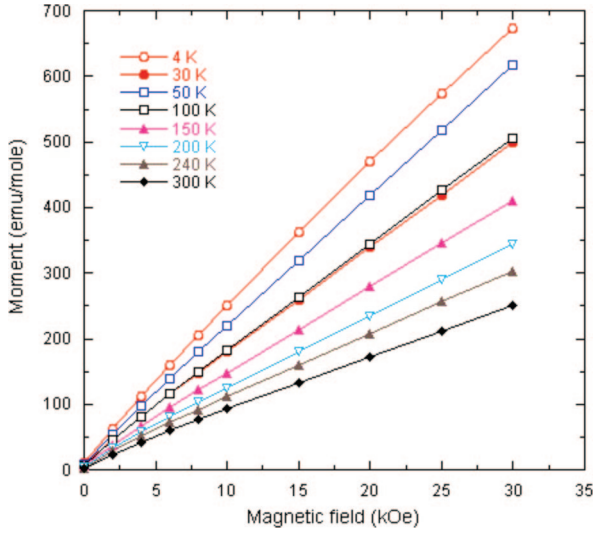

Figure 8. Same as Figure 7 for the L005 sample.

The common feature of the samples prepared with Li deficiency is the nonlinear variation of the magnetization $M(H)$ illustrated in Figures 7 and 8. This nonlinearity is linked to a superparamagnetic contribution of an impurity phase that takes place at a temperature close to 215 K, which is the signature of Fe_2P nanoparticles that order ferromagnetically at this temperature.[30] Another means to give evidence of the presence of this impurity is to plot H/M measured in field $H = 30$ kOe as a function of temperature. These curves, reported in Figures 9 and 10 for the L004 and L005 samples, show a deviation from the linear behavior above 210 K, due to the fact that the contribution of the Fe_2P nanoparticles above this temperature is strongly reduced by the transition of Fe_2P to the paramagnetic phase. Because the slope $\chi = dM/dH$ of the magnetization curves of Fe_2P at 30 kOe is small in the ferromagnetic phase, χ is a good estimate of the intrinsic part of the susceptibility. The values

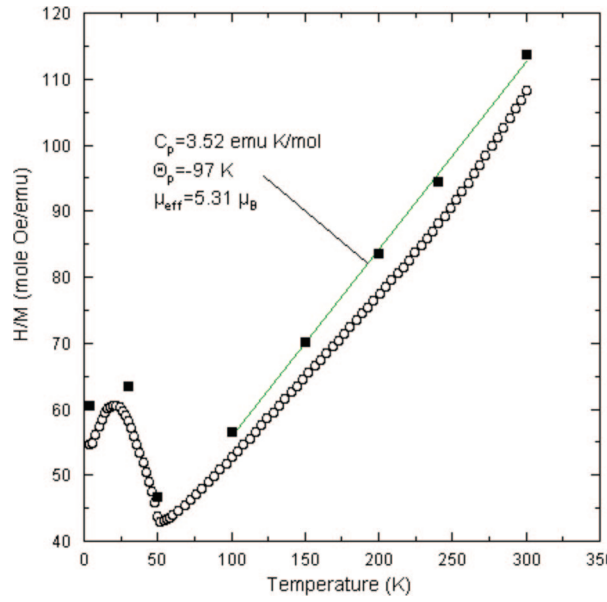

Figure 9. Inverse of the magnetic susceptibility of L004 sample as a function of temperature. The "○" are experimental data of H/M, where M is the magnetization measured in field $H = 30$ kOe. The "■" are the values of $(dM/dH)^{-1}$, where dM/dH is the slope of the magnetization curves in Figure 7 measured at $H = 30$ kOe, to subtract the spurious effects of the Fe_2P impurities.

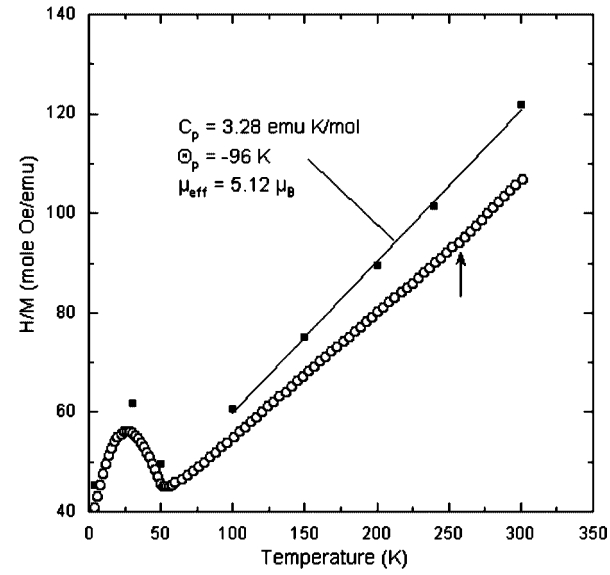

Figure 10. Temperature dependence of the inverse of the magnetic susceptibility at $H = 30$ kOe, for the L005 sample after subtraction of its sarcopside impurity as explained in the text. The "○" are experimental data of H/M measured in field $H = 30$ kOe. The "■" are the values of $(dM/dH)^{-1}$, where dM/dH is the slope of the magnetization curves in Figure 8 measured at $H = 30$ kOe to subtract the spurious effects of the Fe_2P impurities.

of χ^{-1} thus obtained are also reported in Figures 9 and 10. Indeed, the Curie−Weiss law is recovered in this process, which allows us to estimate the effective moment carried by iron in the matrix. The result is $\mu_{eff} = 5.12\ \mu_B$ for L005 and 5.31 for L004. Note the L005 sample has another impurity phase $Fe_3(PO_4)_2$ that has been identified by XRD (see Table 1). We took it into account only in the concentration of iron ions in the product. Indeed, the iron ions are also in the Fe^{2+} valence state in $Fe_3(PO_4)_2$ and then carry the same magnetic moment. In addition, the magnetic

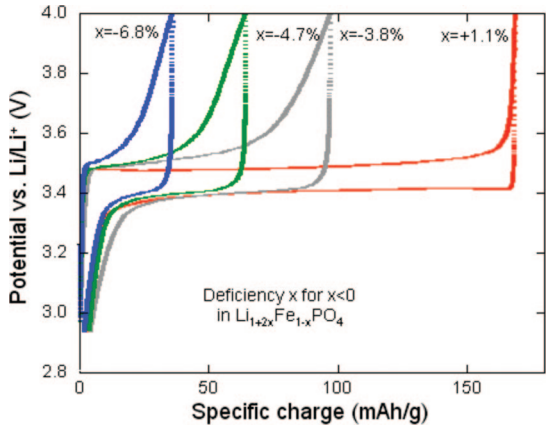

Figure 11. Electrochemical charge/discharge curves (second cycle) of $LiFePO_4$ samples with Li deficiency defined by $Li_{1+2x}Fe_{1-x}PO_4$ for $x < 0$.

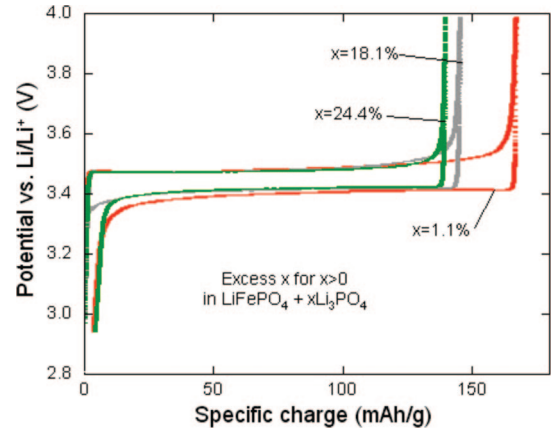

Figure 12. Electrochemical charge/discharge curves (second cycle) of $LiFePO_4$ samples with Li_3PO_4 excess defined by $LiFePO_4 + xLi_3PO_4$ for $x > 0$.

ordering temperature of sarcopside is 44 K,[35] which compares well with that of $LiFePO_4$ so that an iron ion in sarcopside and in $LiFePO_4$ should have the same contribution to the magnetic susceptibility.

Both in L004 and in L005 samples, μ_{eff} is larger than 5 μ_B, which is the signature of magnetic polarons. Let us recall that a magnetic polaron is simply a Li vacancy, the electric neutrality of this defect being ensured by a valence change of an iron ion in its vicinity from Fe^{2+} to Fe^{3+}. We shall then refer to this defect as an isolated Li vacancy, to make a distinction from the complex defect in eq 3 in which the Li vacancy is bound to a $Fe^{\bullet}_{Li}$ antisite defect. The existence of isolated Li vacancies in the L004 and L005 samples is not surprising, because the samples have been prepared with Li deficiency. The important result, however, is that μ_{eff} does not exceed 5.31 corresponding to a concentration of isolated Li vacancies the order of 0.3 mol %,[2] which is very small, and not detectable by any other means but magnetic measurements. This concentration, which is also the typical concentration of magnetic polarons met in different $LiFePO_4$ samples prepared by different techniques, can then be viewed as the saturation limit ε for the amount of isolated Li vacancies that can be formed. This result refines the estimate of ε we had inferred from the analysis of the structural properties. Larger Li deficiency only results in the formation of the defect identified in eq 3. Note the iron ion in this complex $Fe^{\bullet}_{Li} + V'_{Li}$ is in the Fe^{2+} configuration and thus carries the same magnetic moment as iron ions on the (4*c*) Wyckoff lattice sites. This complex is thus undetectable by magnetic measurements, contrary to V'_{Li} alone that generates an additional magnetic moment due to the formation of the magnetic polaron.[4]

3.4. Electrochemical Properties. Charge discharge curves of $LiFePO_4$ phases with formal Li_3PO_4 deficiency and excess are compared in Figures 11 and 12, respectively. For deficient phases, the deviation from the ideal stoichiometry is described by the formula $Li_{1+2x}Fe_{1-x}PO_4$ for $x < 0$. As compared to stoichiometric $LiFePO_4$, we observe a disproportionately high loss of specific charge and discharge capacity. For $x = -3.8$, the lithium content is reduced about 11.4% as compared to ideal stoichiometric $LiFePO_4$. We should expect an equivalent loss of capacity. The observed loss, however, is around 40%. This loss of electrochemical activity cannot be explained by the reduced lithium content in the deficient materials. Furthermore, the charge discharge profiles differ significantly from those of the stoichiometric samples. The flat characteristic of the charge profile is lost, and the voltage hysteresis increases. We have evidenced the presence of a residual amount of Fe_2P impurity in L004 ad L005 samples. This impurity that can lead to Fe diffusion in the electrolyte is known to be damageable to electrochemical properties. Because, however, the amount of Fe_2P is of the order of 0.1 mol %, the main cause for the degradation of the electrochemical properties is unambiguously the defect identified in eq 3. The reason is that the lithium insertion/extraction is essentially a 1D ionic conduction along the Li channels, that is, along the *b* direction (see Figure 1), so that any $Fe^{\bullet}_{Li}$ defect blocks the Li diffusion along the channel where the defect in eq 3 is located. This result is consistent with the high migration energy (0.70 eV) of $Fe^{\bullet}_{Li}$ along this direction.[26]

For materials with Li_3PO_4 excess ($x > 0$), the deviation x of the ideal formula can be described by $LiFePO_4 + xLi_3PO_4$. This description is supported by the results of XRD measurements that clearly indicate the presence of both phases in the excess materials. The quantitative results of the Rietveld refinement are in good correspondence with the data obtained from chemical analysis. As compared to the deficient series even for materials with a high excess of Li_3PO_4, flat voltage profile is not affected and corresponds to that of ideal stoichiometric material. Figure 13 shows the specific capacity of different samples versus the Li_3PO_4 excess in $LiFePO_4$. Even for high x, the experimental data fit to the theoretical values calculated from ICP and XRD. So the effect of Li_3PO_4 excess on the discharge capacity can be interpreted as a dilution of the active material by electrochemically inactive Li_3PO_4. If we remove from the mass of the L028 sample the inert mass of the Li_3PO_4, the theoretical capacity of $LiFePO_4$ is recovered, which is consistent with the fact that both structural and magnetic properties show that there is no defect and no impurity (besides Li_3PO_4) in this sample. The lithium phosphate is then an inert mass with respect to electrochemical properties.

(35) Ericsson, T.; Nord, A. G. *Am. Mineral.* **1984**, *69*, 889.

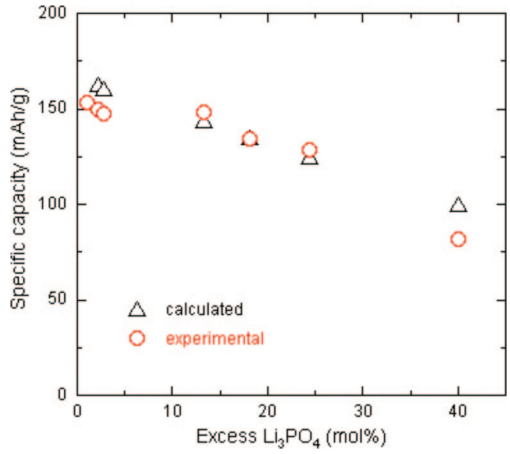

Figure 13. Specific capacity versus excess of Li_3PO_4 in $LiFePO_4$ electrode materials.

4. Conclusion

The study of Li-rich and Li-deficient $LiFePO_4$ samples provides insight into defect properties in relation to the electrochemical performance of this material as a cathode element of Li-ion batteries. The main conclusions can be summarized as follows.

(a) There is a strong dissymmetry in the Li−Fe exchange of ions; up to a few at. % Fe on Li sites can be observed, but not Li on Fe sites.

(b) The antisite $Fe^{\bullet}_{Li}$ that is observed in Li-deficient samples is not isolated and is coupled to a Li vacancy to form a complex defect $Fe^{\bullet}_{Li} + V'_{Li}$. This result is consistent with a recent theoretical work, according to which there is a large binding energy between $Fe^{\bullet}_{Li}$ and V'_{Li}. This defect strongly degrades the electrochemical performance, the Fe ion on the lithium site preventing the 1D-migration of the corresponding Li channel, which confirms the large migration energy of this defect.[26]

(c) The limit of dilution for the $Fe^{\bullet}_{Li} + V'_{Li}$ defects is 6 at. %. Above this limit, these defects aggregate to form sarcopside precipitates. This gives evidence of the negative binding energy of the $Fe^{\bullet}_{Li} + V'_{Li}$ defects. This feature suggests that, in the range of concentrations for such defects $x < 6$ at. %, aggregates of $Fe^{\bullet}_{Li} + V'_{Li}$ can be formed at the atomic scale as precursor of the larger sarcopside clusters formed as soon as $x = 6$ at. %. In particular, this result provides some enlightenment on the recent observation of the aggregation of $Fe^{\bullet}_{Li}$ at this atomic scale by TEM for a defect concentration of 1 at. %.[27]

(d) We found it impossible to generate $Li^{\bullet}_{Fe}$ defects, any excess in Li in the synthesis process leading to the formation of Li_3PO_4 impurity that simply acts as an inert mass in the electrochemical properties of the material.

Attention must be then paid in the preparation process of $LiFePO_4$ to avoid deviations from stoichiometry, in particular Li deficiency.

CM803408Y